Contrib Mineral Petrol (1994) 118:130–137

Mark I. Pownceby · Hugh St.C. O'Neill

Thermodynamic data from redox reactions at high temperatures. IV. Calibration of the Re-ReO_2 oxygen buffer from EMF and NiO + Ni-Pd redox sensor measurements

Received: 29 June 1993 / Accepted: 26 May 1994

Abstract The chemical potential of oxygen defined by the equilibrium:

$$Re(solid) + O_2(gas) = ReO_2(solid)$$

has been measured between 850 and 1250 K via an electrochemical method using calcia-stabilized zirconia electrolytes and either Ni + NiO or Cu + Cu_2O as the reference electrode. The results are:

$$\mu O_2^{Re+ReO_2}(\pm 400) = -451020 + 297.595\ T - 14.6585\ T \ln T \quad (850 < T < 1250)$$

where μO_2 is in $J \cdot mol^{-1}$, T in kelvins, and the reference pressure for O_2 is 1 bar (10^5 Pa). (Values in terms of log-f_{O_2} may be obtained from the above expression by dividing by $RT\ln 10$, where $R = 8.31441\ J.K^{-1} \cdot mol^{-1}$). The standard enthalpy of formation of ReO_2 is -444.350 ± 0.400 (1σ) $kJ \cdot mol^{-1}$, requiring a significant modification to previously published estimates. These results were checked in hydrothermal experiments using the double capsule method with NiO + Ni-Pd alloy as an oxygen sensor. Reversals at $P = 1$ kbar over the T range 823 to 1073 K are in good agreement with the electrochemical measurements. These latter results also serve to demonstrate: (1) the usefulness of the "redox sensor" method; (2) the viability of using Re + ReO_2 as a buffer in hydrothermal experiments. Re + ReO_2 lies nearly midway between the Ni + NiO and Fe_3O_4 + Fe_2O_3 buffers in μO_2-T space, and thus fills a petrologically important gap in the range of μO_2s which can be covered by accurately calibrated oxygen buffers.

Mark I. Pownceby (✉)
CSIRO Division of Mineral Products, PO Box 124,
Port Melbourne, Victoria, 3207 Australia.

Hugh St.C. O'Neill
Bayerisches Geoinstitut, Universität Bayreuth, Postfach 101251,
D-95440 Bayreuth, Germany

Editorial responsibility: W. Schreyer

Introduction

Oxygen fugacity is an important variable in petrogenesis, and the control of oxygen fugacity is often necessary in experimental petrology. A simple and effective way to accomplish this in high pressure hydrothermal experiments is by the use of oxygen fugacity buffers (isobarically univariant redox equilibria) in the "double capsule" method (Eugster 1957; Eugster and Wones 1962; Huebner 1971; Chou 1987). In this approach, two or more solid phases (for example, simple metal plus metal oxide assemblages) react to maintain (buffer) the oxygen fugacity of an aqueous fluid, usually water, at a constant value. The method depends on the availability of a suit-

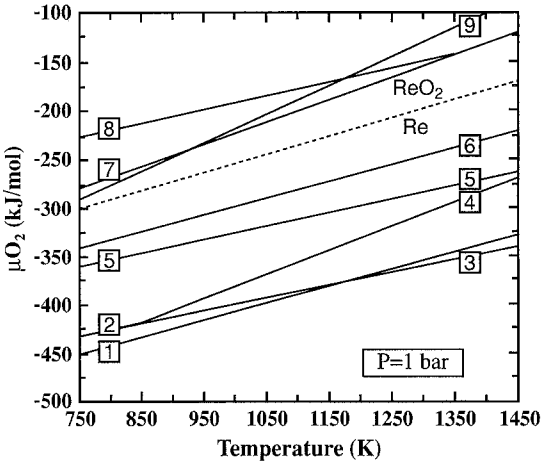

Fig. 1 μO_2 versus temperature diagram showing the relative positions of the commonly used oxygen fugacity buffers. The Re + ReO_2 equilibrium (*dashed line*) lies approximately mid-way between the Ni + NiO and Fe_3O_4 + Fe_2O_3 buffers. [Key to numbering: 1 W + WO_2 (O'Neill and Pownceby 1993a), 2 Fe + Fe_3O_4 (O'Neill 1988), 3 Fe + "FeO" (O'Neill and Pownceby 1993a), 4 "FeO" + Fe_3O_4 (O'Neill 1988), 5 Co + CoO (O'Neill and Pownceby 1993a), 6 Ni + NiO (O'Neill and Pownceby 1993a), 7 MnO + Mn_3O_4 (O'Neill and Pownceby 1993b), 8 Cu + Cu_2O (O'Neill and Pownceby 1993a), 9 Fe_3O_4 + Fe_2O_3 (Hemingway 1990)

able buffer of the desired oxygen fugacity. Whilst the present supply of oxygen buffers enables a broad range of μO_2 to be covered (Fig. 1), the buffers themselves are limited to discrete, discontinuous steps in T versus μO_2 space. In many cases there are large gaps present between μO_2s defined by individual buffer assemblages – for example Fig. 1 illustrates there is a difference of around 50–75 kJ·mol^{-1} (approximately 3–4 log-bar units in f_{O_2}) between the Ni + NiO (NNO) buffer, and a group of three buffers at more oxidizing conditions; the Fe_3O_4 + Fe_2O_3 (HM), Cu + Cu_2O and MnO + Mn_3O_4 (MNO) buffers. This is the region of f_{O_2} in which most acid igneous rocks have crystallized (Carmichael 1991), and in which many metamorphic rocks equilibrated. It would therefore be advantageous to have a new buffer assemblage to enable experimentation at these intermediate oxygen fugacities.

Available thermochemical data (e.g. Pankratz 1982) show that a buffer based on the reaction:

$$Re(s) + O_2(g) = ReO_2(s) \quad (s = \text{solid}, g = \text{gas}) \qquad [1]$$

(hereafter designated RRO), should prove to be a new oxygen buffer assemblage lying approximately midway between the NNO and MNO buffers (see Fig. 1). Existing data for the Re + ReO_2 equilibrium come from three types of measurements. Firstly, there are complete calorimetric data for both Re and ReO_2: low temperature heat capacities down to 0.16 K for Re (Hultgren et al. 1973) and to 5 K for ReO_2 (Stuve and Ferrante 1976), high temperature heat content measurements to 1474 K for Re (Hultgren et al. 1973) and to 1400 K for ReO_2 (Stuve and Ferrante 1976), and the heat of formation of ReO_2 (King et al. 1969). The uncertainty of this latter value is quoted as ± 3.3 kJ·mol^{-1}, which translates into an uncertainty for the RRO oxygen buffer of 0.2 log-bar units in f_{O_2}. This is rather more than is desirable for an oxygen buffer: the other commonly used buffers shown in Fig. 1 are mostly known to an accuracy of ± 0.02 log-bar units (e.g. O'Neill and Pownceby 1993a).

Secondly, thermochemical data for the Re oxides (ReO_3 and Re_2O_7 as well as ReO_2) have been presented by several authors from vapour pressure measurements, including the disproportionation-volatilization reaction:

$$7ReO_2(s) = 3Re(s) + 2Re_2O_7(g) \qquad [2]$$

(e.g. Battles et al. 1968). These studies, which do not claim great accuracy, show a wide dispersion in results. The extraction of thermochemical data for ReO_2 also depends on estimated data for Re_2O_7(g). Nevertheless, the values given by Battles et al. (1968) are in reasonable agreement with the calorimetric data. The other work is critically discussed by King et al. (1969) and Stuve and Ferrante (1976), and will not be considered further.

Thirdly, the μO_2 for RRO has been measured by Franco and Kleykamp (1971) using an electrochemical technique with calcia-stabilized zirconia (CSZ) as the solid electrolyte. Franco and Kleykamp used the "open sandwich" experimental arrangement, in which the sample and reference electrodes are separated only by a disc of the electrolyte, and both electrodes are subjected to the same stream of inert gas. They used Fe + "FeO" as the reference electrode. The large difference in the μO_2 of this electrode from Re + ReO_2 could cause problems with this method (e.g. Ramanarayanan 1980), and for RRO, further problems can be expected because of the tendency of ReO_2 to decompose by disproportionation and volatilization, according to reaction [2]. These problems might be reflected in the poor precision of ± 2.2 kJ·mol^{-1} in the measurements reported by Franco and Kleykamp (that is, compared to other similar high temperature electrochemical studies, see for example O'Neill and Pownceby 1993a), although their results appear to be in surprisingly good agreement with the calorimetric data.

We have therefore undertaken to re-calibrate the RRO oxygen buffer over the temperature range 850–1250 K using a precise electrochemical method (O'Neill and Pownceby 1993a) with closed gas-tight electrode compartments. Despite this, we found the volatility of ReO_2 (Eq. [2]), still presented a problem. Accordingly, we have also determined the RRO buffer using a hydrothermal double capsule method with NiO + Ni-Pd as a "redox sensor" (Taylor et al. 1992). These experiments also serve to demonstrate: (1) the usefulness of the "redox sensor" method; (2) the viability of using RRO as a buffer in hydrothermal experiments.

Experimental methods and strategy

EMF measurements

Electrochemical cells of the type:

$$Pt, M + M_xO \mid CSZ \mid Re + ReO_2, LaCrO_3, Pt \qquad [I]$$

where M = Cu or Ni, were constructed as described in O'Neill and Pownceby (1993a). Under ideal conditions (e.g. zero electronic conductivity) the open circuit EMF, E, developed by such a cell is related to the difference in μO_2 between the two electrodes by:

$$4FE = \mu_{O_2}^{RRO} - \mu_{O_2}^{MMO} \qquad [3]$$

where F is the Faraday constant (96 484.56 coulomb·mol^{-1}). As the method measures the difference between the chemical potentials of the two electrodes, one, with known μO_2, must be chosen as the reference. Additionally, since a potential problem in EMF work is the possible transfer of oxygen from the electrode with the higher μO_2 to the other, it was considered desirable to bracket the RRO equilibria by doing two sets of experiments, one with a reference electrode with higher μO_2, and another with a lower. In this study, Ni + NiO mixtures were used for the lower μO_2 reference electrode and Cu + Cu_2O was used as the higher μO_2 electrode. The μO_2 values defined by the Ni + NiO and Cu + Cu_2O equilibria have recently been re-calibrated in this laboratory (O'Neill and Pownceby 1993a) and are taken to be (μO_2 in J·mol^{-1}; T in kelvins):

$$Cu + Cu_2O: \mu O_2 (\pm 80) = -347\,705 + 246.096\,T - 12.9053\,T\ln T \quad (700 < T < 1338) \qquad [4]$$

$$Ni + NiO: \mu O_2 (\pm 200) = -478\,967 + 248.514\,T - 9.7961\,T\ln T \quad (700 < T < 1700) \qquad [5]$$

Table 1 Lattice parameters and molar volumes of Re and ReO_2 from samples before and after EMF measurements

Sample	ReO_2 (Orthorhombic)				Re (Hexagonal)		
	a_0	b_0	c_0	$V^{\circ}_{298,1\,bar}$ [a]	a_0	c_0	$V^{\circ}_{298,1\,bar}$ [a]
1) Before EMF measurements (Cu $K_{\alpha 1}$ radiation)[b]:							
(973 K/1kb)	4.8073(3)	5.6413(2)	4.5992(2)	1.8779	2.763(1)	4.458(2)	0.887
2) After EMF measurements (Co $K_{\alpha 1}$ radiation):							
Ni #1	4.8075(3)	5.6414(2)	4.5991(3)	1.8779	2.7606(3)	4.4589(4)	0.8862
Cu #1	4.8071(3)	5.6411(2)	4.5997(2)	1.8779	2.7608(3)	4.4586(5)	0.8862
For comparison, lattice parameters given by Magnéli (1957) are:							
	ReO_2	$a_0 = 4.8094(35)$		$b_0 = 5.6433(5)$		$c_0 = 4.6007(5)$	
	Re	$a_0 = 2.762(1)$		$c_0 = 4.457(1)$			

[a] molar volume in $J \cdot bar^{-1}$
[b] ReO_2 with minor amount of Re was synthesized at 1.0 kb and 973 K for ~48 h. (see text for details)

The reference pressure for oxygen is 1 bar (10^5 Pa), and the uncertainty given in parentheses is one standard deviation.

Temperatures were measured to ± 0.1 K with Pt-$Pt_{90}Rh_{10}$ thermocouples calibrated against the melting point of gold using the IPTS-90 scale. Temperatures are reported to the nearest degree to allow for errors in calibration and measurement. The cell EMFs were measured to the nearest ± 0.01 mV, and have been reported to the nearest 0.1 mV. The performance of all cell assemblies was checked by measuring the EMF of symmetrical cells of the type:

$$Pt, M + M_xO \mid CSZ \mid M + M_xO, LaCrO_3, Pt \qquad [II]$$

where M = Fe, Co, Ni or Cu (see O'Neill and Pownceby 1993a).

Starting materials

The metal-metal oxide reference electrodes for the EMF experiments were made from mixtures of Cu and Cu_2O and Ni and NiO in the approximate molar ratio 3:1. All reagents were stated by the manufacturers to be 99.9% purity or greater. The metals were used as supplied, in the powder form with grain size less than 10 μm. The Cu_2O was prepared from Cu and CuO, mixed in the appropriate proportions but with a slight excess of metal and sintered at 1273 K for ~ 12 hours under a flowing stream of Ar. The NiO was sintered in air at 1273 K for ~ 24 hours; this treatment causes a change in colour from greenish black to bright emerald green and XRD analysis of the sintered material gave a pattern corresponding to well-crystallized NiO.

The Re + ReO_2 pellets were prepared from fine grained (< 1 μm) Re metal powder (99.9%) and ReO_2, also supplied in the form of a fine grained powder (99.99%). Examination by powder XRD revealed the ReO_2 starting material, as supplied, to be a two-phase mixture of the low temperature monoclinic form and the high temperature orthorhombic form, which is the form of interest in this study. The XRD reflections from the monoclinic polymorph were noticeably broadened, indicating very fine grain size. Although Magnéli (1957) has reported that the monoclinic form of ReO_2 will transform to the orthorhombic form at a temperature as low as 580 K, it was felt that it would be advantageous to begin the cells with as well-crystallized ReO_2 as possible, not least to minimize vaporization (Eq. [2]). Accordingly, the ReO_2 was hydrothermally re-crystallized. Approximately 0.5 g aliquots of the ReO_2 were sealed with a small amount of water into Ag capsules, and run at 973 K, 1.0 kbar for ~ 48 hours in a conventional Tuttle bomb with H_2O as the pressure medium. The products consisted of well-crystallized, orthorhombic ReO_2 which gave very sharp XRD reflections, plus a small amount of Re metal. The presence of the metal indicates that the f_{O_2} of the pressure vessel is slightly below that of the RRO buffer.

Accurate unit cell parameters were collected using a Stoe STADIP automated powder diffractometer using either $CuK_{\alpha 1}$ (λ = 1.54056 Å) or $CoK_{\alpha 1}$ (λ = 1.78897 Å) radiation. All samples were measured with an internal standard of NBS Silicon (a_o = 5.43094). Results are given in Table 1, together with XRD data for the Re + ReO_2 pellets determined after the EMF measurements. The unit cell parameters for ReO_2 are in reasonable agreement with the study of Magnéli (1957). Battles et al. (1968) report that the unit cell parameters of ReO_2 are the same whether equilibrated with either excess Re or excess ReO_3, indicating that the range of homogeneity of ReO_2 must be quite narrow, but do not give further details.

Performance of the electrochemical cells

The RRO runs approached equilibrium sluggishly taking 4 days at ~ 973 K to reach a steady-state EMF. After reaching a stable EMF, the cells were then left at the initial temperature for a further 24 hours before the first reading was recorded, by which time the EMF had been observed to be stable to within ± 0.2 mV and with no detectable drift for at least 12 hours. The EMF reacted slowly to temperature changes requiring ~ 36 hours to equilibrate at 850 K and ~ 8–10 hours at 1200 K. Nevertheless, consistent data could be obtained after both increasing and decreasing temperature. Recorded values were always within ± 0.5 mV after heating and cooling cycles. Total run times were of the order of 30–35 days. The range of temperature covered is from 850 K, the lowest temperature at which equilibrium can be attained in a reasonable amount of time, to 1250 K, above which the vapour pressure of Re_2O_7 becomes prohibitively high.

Examination of all three cells after the EMF runs showed evidence for substantial transport of Re oxides from the Re + ReO_2 electrode pellet. The inside of the CSZ tube and the outside of the alumina push rod (see Fig. 1 in O'Neill and Pownceby 1993a) were coated with a mottled, bluish-black and dark-mauve material, in places thick enough to flake off. This material extended some 15 cm upwards from the hotspot of the furnace, to where the temperature could only have been a few hundred degrees Celsius. Much of this material could be washed off with water. Although we did not analyse this material, we believe it to be Re_2O_7 perhaps with other oxides of Re, formed by the disproportionation-volatilization according to Reaction [2] above, and transported out of the hot zone of the furnace. Ultimately, this disproportionation-volatilization reaction would deplete the electrode in ReO_2, although examination of the electrodes after each run by powder XRD revealed that substantial ReO_2 (and Re) still remained after all three runs.

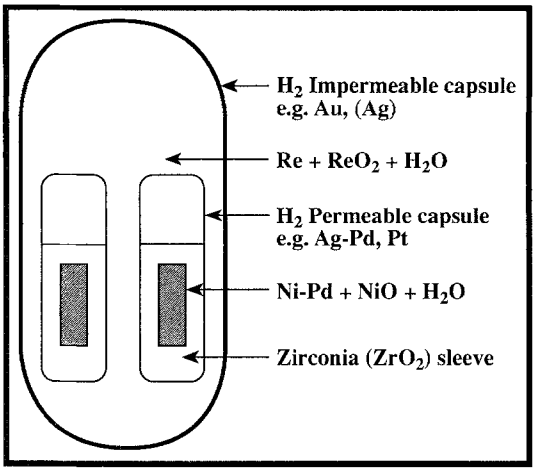

Fig. 2 Schematic diagram of the NiO + Ni-Pd redox sensor experimental arrangement used to determine the position of the Re + ReO_2 equilibrium. See text for explanation of loading method, capsule materials and NiO + Ni-Pd sensor compositions

Redox sensor measurements

Recent investigations by Taylor et al. (1992) have shown that using simple binary metal alloy or oxide solid solutions is a powerful technique for accurately measuring oxygen fugacity in hydrothermal experiments. We have used the redox sensor method to calibrate Reaction [1] using experimental procedures similar to those detailed in Taylor et al. (1992). The equilibrium μO_2 of Reaction [1] lies approximately mid-way between that defined by the NNO and HM buffers and is thus readily accessible using the NiO + Ni-Pd redox sensor, which we have re-calibrated recently (Pownceby and O'Neill 1994). Using the results from the EMF experiments, NiO + Ni-Pd starting compositions lying either side of the composition predicted for the μO_2 of the RRO buffer were prepared so that the compositions could converge, generating a reversal.

Sensor charges were prepared from fine grained ($\sim$ 1 μm), analytical grade Ni and Pd powders (grainsize $<$ 1–1.5 μm and purity $>$ 99.9%), mixed in the appropriate stoichiometric proportions. An excess of NiO powder (in the approximate molar ratio 3:1, Ni-Pd:NiO) was added to all mixtures. Each sensor composition was packed into a pre-fabricated, porous, ZrO_2 cylinder which was then loaded into a Pt capsule (2.0 mm OD, 1.8 mm ID and 10 mm in length). A small amount of powdered ZrO_2 was then added to cover the sample. The ZrO_2 effectively acts as an inert barrier to prevent the Ni-Pd metal of the sensor alloying with the capsule wall material. Approximately 3–4 μl water was added to the charge which was then arc-welded shut. The two sensor capsules (comprising a reversal pair) were flattened down to a point just above the ZrO_2 tube using a pair of pliers and then placed with the oxygen buffer ($\sim$ 1:1 Re:ReO_2 molar proportions) and 30–50 μl H_2O into a Au capsule (5.0 mm OD, 4.5 mm ID, 30 mm long), which was then welded shut. In this arrangement, we are using the Ni-Pd alloy as an f_{H_2} sensor, relying on the diffusion of H_2 through the Pt capsule walls to effect a compositional readjustment. Capsules were tested for possible leaks by heating in an oven at $\sim$ 500 K for 2–3 hours. The entire experimental arrangement is shown schematically in Fig. 2.

Experimental apparatus

Conventional 300 mm (length) × 40 mm (OD) × 6.5 mm (ID) cold-seal pressure vessels were used for the hydrothermal runs at temperatures between 823 and 1173 K. Water was used as the pressure medium. Using water imparted an added experimental advantage as NIMONIC 105 alloy pressure vessels buffer oxygen fugacity at conditions slightly more oxidizing than NNO (Kerrick 1987). Since the predicted location of the RRO buffer lies within this region, there will be minimal f_{H_2} gradient between charge and bomb, enabling runs of long duration (e.g. 931 h at 873 K) to be performed.

In order to minimize temperature gradients and possible convection, the pressure vessels were placed horizontally (e.g. Rudert et al. 1976) in split furnaces with a 20 mm (length) × 5.0 mm (diam.) nickel filler rod resting against the charge. An external thermocouple was used to monitor the temperature during each experiment and was checked against a standard thermocouple at periodic intervals. The cold-seal vessels were probed with a sheathed chromel-alumel thermocouple at 1 atm. and 1.0 kbar to examine longitudinal thermal gradients. The determination showed a maximum gradient of 3–4 K over the sample in the pressure vessels. Additionally, no radial gradients were found across the hot zone of the bomb with the charge in place. Reported temperatures are therefore believed accurate to $\pm$ 5 K and pressures accurate to $\pm$ 50 bars. Note that the Ni-Pd alloy composition corresponding to the μO_2 of the RRO buffer is relatively insensitive to temperature, so that these uncertainties in T translate into relatively minor uncertainties in measured μO_2. The entire pressure-vessel sample assemblage was quenched by a stream of compressed air.

Phase characterization

At the completion of the hydrothermal runs the buffer capsules were weighed, carefully punctured, and then dried to verify the presence of water. For all charges the mass had slightly increased indicating that hydrogen had diffused into the capsule, consistent with the f_{O_2} of the bomb being below that of the RRO buffer. The XRD analysis of the Re + ReO_2 assemblage confirmed the presence of both buffer components, with an increase in the amount of Re relative to ReO_2. There was no obvious reaction of the buffer with the Au capsule.

The small amount ($\approx$ 20 mg) of Ni-Pd alloy in the sensor capsules proved impossible to extract. Instead, sensor capsules were punctured and dried before mounting entirely within epoxy resin. These mounts were then carefully sectioned to fully expose the sensor, before being polished flat for examination by reflected light optical microscopy, and electron microprobe analysis. This procedure has the advantage of: (1) providing a profile of the sensor charge permitting visual inspection as to whether the Ni-Pd had breached the zirconia jacket and contacted with the capsule walls; (2) exposing a broad area of alloy enabling the entire length of the charge to be examined for homogeneity.

Microprobe analysis of the Ni-Pd solid solutions was performed using a Cameca SX-50 electron microprobe equipped with wavelength dispersive LIF and PET crystal spectrometers. Nickel and palladium wire (both 99.99 + %) were used as standards. An accelerating potential of 15 kV, a sample current of 15 nA and a beam diameter of 2–4 μm were standard operating conditions. Counting times were sufficient to collect $>$ 50000 counts in standards and unknowns. The Ni-Pd alloy commonly formed interconnecting blebs of metal whereas NiO was present as fine grained interstitial material. There was no obvious reaction of the external RRO buffer with the Pt sensor capsule. Approximately 25–35 analyses were performed on each pellet revealing complete homogenization of the alloy (to within about $\pm$ 0.3–0.5 mol% X_{Ni}). Electron microprobe results are summarized in Table 3.

Table 2 Experimental results from the cells used to measure the free energy of formation of ReO_2. The order is that in which the measurements were made. Temperatures and EMF's are considered accurate to ± 0.5 K and ± 0.2mV respectively

T (K)	EMF (mV)	$-\mu O_2$ (kJ mol^{-1})	T (K)	EMF (mV)	$-\mu O_2$ (kJ mol^{-1})	T (K)	EMF (mV)	$-\mu O_2$ (kJ mol^{-1})	T (K)	EMF (mV)	$-\mu O_2$ (kJ mol^{-1})
Run Ni #1: Re + ReO_2 vs. Ni + NiO											
963.0	110.3	261.88	920.5	109.4	269.55	1004.9	111.5	254.27	1108.4	114.3	235.53
941.6	110.0	265.66	941.5	109.8	265.75	1026.0	112.4	250.32	1087.0	113.8	239.35
920.7	109.7	269.40	963.0	110.7	261.75	1046.6	112.9	246.57	1067.4	113.4	242.86
899.8	109.3	273.11	920.7	110.0	269.29	1067.5	113.3	242.86	1046.5	112.8	246.64
879.2	109.0	276.81	879.1	109.2	276.72	1087.1	113.7	239.37	1025.5	112.7	250.28
856.9	108.5	280.83	900.2	109.5	272.99	1108.5	114.2	235.53	1067.3	113.3	242.93
834.8	107.9	284.86	920.9	109.8	269.34	1128.9	114.7	231.88	1108.2	114.2	235.58
857.0	108.3	280.91	942.0	110.1	265.57	1148.7	115.2	228.33	1148.5	115.2	228.36
879.2	108.7	276.93	963.3	110.6	261.75	1169.2	115.7	224.69	1190.1	116.3	220.90
899.8	109.0	273.25	984.4	111.0	257.94	1128.9	114.8	231.86			
Run Cu #1: Re + ReO_2 vs. Cu + Cu_2O											
920.2	171.8	268.59	920.1	171.8	268.63	1086.4	156.0	238.57	1127.8	152.0	231.12
899.6	173.6	272.28	941.0	169.9	264.83	1045.5	160.3	246.06	1147.5	150.3	227.67
878.9	175.5	276.01	962.0	167.9	261.05	1003.8	164.3	253.60	1167.7	148.2	223.98
856.4	177.2	279.96	983.8	165.9	257.10	961.8	168.0	261.10	1188.9	146.4	220.27
834.6	178.7	283.75	1004.1	163.9	253.41	983.2	166.3	257.38	1107.1	153.6	234.69
856.6	177.3	279.98	1024.8	161.8	249.65	1024.2	162.4	249.96	1085.6	155.3	238.41
878.5	175.6	276.11	1045.8	159.9	245.87	1066.3	158.0	242.23	1188.9	146.5	220.31
899.3	173.7	272.36	1066.6	157.8	242.07	1107.2	154.1	234.87			
Run Cu #2: Re + ReO_2 vs. Cu + Cu_2O											
1005.1	165.0	253.70	877.6	177.6	277.03	1087.4	156.9	238.76	1189.4	147.0	220.43
984.3	167.0	257.48	899.6	175.2	272.88	1107.0	154.9	235.21	1148.3	151.1	227.83
962.6	169.0	261.39	921.0	172.7	268.85	1148.5	150.9	227.73	1168.4	149.1	224.22
941.9	170.8	265.08	941.9	170.6	264.98	1107.0	154.9	235.21	1189.3	147.1	220.47
921.1	172.6	268.78	962.4	168.7	261.27	1066.5	158.9	242.54	1209.6	145.1	216.85
899.7	174.6	272.64	984.1	166.7	257.38	1025.1	162.7	249.94	1229.7	143.2	213.26
877.9	177.2	276.85	1005.1	164.7	253.60	1045.3	161.0	246.38	1250.3	141.4	209.63
857.0	179.2	280.64	1025.5	162.7	249.89	1087.1	156.9	238.82	1229.8	143.5	213.34
835.7	181.7	284.75	1045.7	160.9	246.28	1127.8	153.0	231.47	1209.5	145.4	216.96
857.0	179.8	280.86	1066.4	158.9	242.56	1168.5	149.0	224.17	1127.1	153.2	231.66

Results and discussion

Electrochemical cells

The results from three cells, one with Ni + NiO and two with Cu + Cu_2O as the reference electrodes, are given in Table 2, and are plotted relative to the values from Pankratz (1982) as a function of temperature in Fig. 3. Since the values in Pankratz (1982) are computed from the calorimetric data, this procedure is equivalent to a third law analysis (e.g. O'Neill and Pownceby 1993b). In particular, a horizontal array on such a plot indicates agreement with the entropy and heat capacity data for the reaction. The values in Pankratz (1982) are well described in the temperature range 600 to 1400 K by the three-term equation:

$$\mu O_{2\,(\text{Pankratz})}^{\text{Re}+\text{ReO}_2} = -455\,613 + 297.595\,T - 14.6585\,T\ln T \quad (\text{in J}\cdot\text{mol}^{-1}) \qquad [6]$$

Figure 3 shows that the three runs show a variation between each other, which is unexpectedly large compared to the accuracy to which other similar electrochemical cells customarily aspire (see O'Neill and Pownceby 1993a), and which is larger than the internal

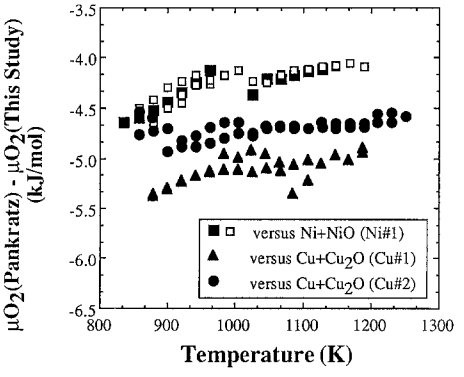

Fig. 3 Comparison of the results for the free energy of the reaction Re + O_2 = ReO_2 from the three EMF experiments in this study, with those derived from the calorimetric data as assessed in Pankratz (1982). Note that at each temperature at least two data points were recorded, representing EMFs measured during the heating *and* cooling cycles. For the sake of clarity, this information is shown only for the experiment Ni #1, where EMFs recorded during the heating cycle are indicated by the *unfilled boxes*; the down temperature cycle results are represented by the *filled boxes*

variation within each run. The reason for this is not known; one speculation is that the volatility problem and the resulting transport of Re to other parts of the cell, with the precipitation of higher oxides (Re_2O_7 and ReO_3), may result in "mixed potentials" due to metastable reactions involving the higher oxides. However, the discrepancies appear to remain constant for the entire duration of each run, although it is expected that the volatilization/re-precipitation would be a time-dependent effect.

Because of this variation we do not attach any significance to the small positive slopes seen in the data from two of the runs in Fig. 3. Rather, we will accept the Pankratz (1982) calorimetric entropies and heat capacities for the reaction, and use our data to refine $\Delta_r H°_{298,1\ bar}$ for Reaction [1] (which is $\Delta_f H°_{298,1\ bar}$ for ReO_2). The three runs give: (Cu #1) = − 443.862 ± 0.227, (Cu #2) = − 444.331 ± 0.111 and (Ni #1) = − 444.760 ± 0.214 kJ·mol^{-1}, with an overall mean $\Delta_f H°_{298,1\ bar}$ of − 444.350 ± 0.400 kJ·mol^{-1} (the uncertainties given are one standard deviation and include those given for the reference electrodes). This value is ~ 4.6 kJ·mol^{-1} less negative than the calorimetric determination of King et al. (1969), a discrepancy which may perhaps be explained if the amount of unreacted Re in the sample of ReO_2 used by King et al. (1969) was ~ 8% rather than the 5% estimated from the chemical analysis (see King et al. 1969, p. 3). We use our new value to amend the expression for the μO_2 (in J·mol^{-1}) of the RRO buffer (Eq. [6]) to:

$$\mu O_2^{Re+ReO_2}(\pm 400) = -451020 + 297.595\ T - 14.6585\ T\ln T \quad [7]$$

Values in terms of $\log f_{O_2}$ may be obtained from the above expression by dividing by $RT\ln 10$, where $R = 8.31441$ J.K^{-1}·mol^{-1}.

Redox sensor measurements

Results from the NiO + Ni-Pd hydrothermal sensor experiments over the temperature range 800 to 1073 K are given in Table 3. Values of μO_2 for each redox sensor pair have been calculated according to the expression:

$$\mu = \mu_{O_2}^{NNO} - 2RT\ln X_{Ni}^{alloy} - [2\cdot(1 - X_{Ni}^{alloy})^2\cdot[(-2165 - 7.958.T) + (9409 - 0.888.T)\cdot(4X_{Ni}^{alloy} - 1) + 2089\cdot(6X_{ni}^{alloy} - 1)\cdot(2X_{Ni}^{alloy} - 1)]] \quad [8]$$

given by Pownceby and O'Neill (1994). The NiO + Ni-Pd redox sensor expression has been corrected for the effects of elevated temperatures and pressures using the data provided in Pownceby and O'Neill (1994). We have been unable to find any equivalent thermal expansion

Table 3 Summary of experimental conditions and results from the hydrothermal NiO + Ni-Pd redox sensor experiments.

Run no.	Initial sensor composition (X_{Ni})	Temperature (± 5 K)	Pressure (± 50 bars)	Run time (hours)	Final sensor composition (X_{Ni})[a]	Number of analyses (EMPA)	μO_2 (kJ/mol)[b]	$\mu O_2^{Re+ReO_2}$ (kJ/mol)[d]
12	0.10	823	1240	869.5	0.1578(34)	24	−286.0	−287.1
	0.25				0.2091(40)	33	−293.5	
13	0.10	848	1205	870	0.1626(41)	31	−281.4	−282.4
	0.25				0.2001(50)	28	−287.1	
11	0.20	873	1025	166	0.1887(42)	23	−280.3[c]	−277.9
	0.30				0.2254(33)	26	−285.4[c]	
4	0.10	873	1075	329.5	0.1674(30)	26	−276.9	−277.9
	0.25				0.2191(46)	35	−284.5	
14	0.10	873	1215	931	0.1656(28)	31	−276.6	−277.9
	0.25				0.1723(47)	37	−277.6	
10	0.10	923	970	124	0.1685(25)	18	−266.5	−268.7
	0.25				0.2131(46)	25	−273.4	
6	0.10	923	1175	316.5	0.1702(34)	18	−266.7	−268.7
	0.25				0.2038(39)	25	−272.0	
9	0.10	973	1100	118	0.1731(43)	28	−256.7	−259.6
	0.25				0.2137(35)	27	−263.1	
17	0.10	973	1100	145.5	0.1823(33)	31	−258.2	−259.6
	0.25				0.1919(31)	26	−259.8	
8	0.10	1023	1100	118	0.1893(27)	38	−248.9	−250.5
	0.25				0.2059(36)	35	−251.6	
5	0.10	1073	1100	72	0.1974(22)	24	−239.8	−241.4
	0.30				0.2048(26)	32	−241.1	
7	0.10	1073	1100	96	0.1972(21)	27	−239.8	−241.4
	0.25				0.2054(28)	27	−241.2	
15	0.10	1073	995	192.5	0.1981(26)	32	−240.0	−241.4
	0.25				0.2044(23)	27	−241.0	

[a] Figures in parentheses indicate the standard deviation (1σ) as determined from the microprobe analyses
[b] Calculated using NiO + Ni-Pd redox sensor expression from Pownceby and O'Neill (1994), and corrected from elevated P to 1 bar
[c] Not a reversal
[d] From Equation [7] in text

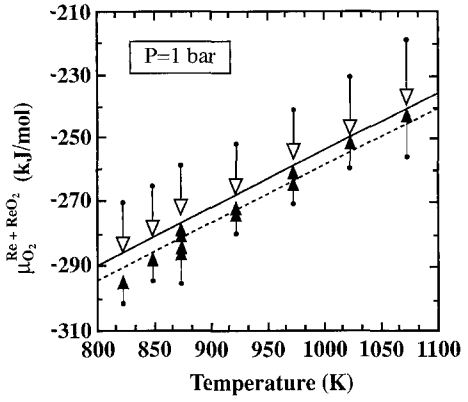

Fig. 4 Results from the hydrothermal NiO + Ni-Pd redox sensor experiments (corrected from elevated P to 1 bar total pressure). *Triangle apices* indicate direction of approach to the equilibrium μO_2. *Filled circles* represent the initial composition of the NiO + Ni-Pd redox sensor expressed in terms of μO_2. *Solid line* is the position of the Re + ReO_2 buffer determined from the EMF measurements (Eq. [6]). The *dashed line* represents the calculated results from Pankratz (1982)

or compressibility data for ReO_2 so, to a first approximation, we have assumed that the pressure dependence of the RRO buffer is simply given by:

$$\int_{1\text{ bar}}^{P} \Delta V^{\circ}_{T,P} \cdot dP = \Delta V^{\circ}_{298,1\text{ bar}} \cdot P = 0.9917 \cdot P \text{ J} \cdot \text{mol}^{-1} \quad \text{(from the data in Table 1).} \quad [9]$$

The NiO + Ni-Pd redox sensor results are represented in Fig. 4 (corrected from elevated P to 1 bar total pressure). Important points which emerge are:

1. At high temperatures (973–1073 K), the reversal brackets are reasonably tight with, in most cases, the sensor compositions converging to within about 0.6–1.0 mol% of each other. At lower temperatures, reversal brackets are not as tightly constrained with these runs approaching, rather than reaching equilibrium. The results indicate that the NiO + Ni-Pd redox sensor approaches equilibrium from more oxidized conditions (low X_{Ni}) considerably more rapidly than from the reverse direction. This could be due to either asymmetry in the rate of reaction of the NiO + Ni-Pd redox sensor, or the difference in the rate of transfer of H_2. Nevertheless, these results still constitute an experimental reversal and provide bounding limits for the Re + ReO_2 equilibrium.

2. The results from the NiO + Ni-Pd redox sensor experiments are in excellent agreement with the equilibrium μO_2 determined from the EMF measurements; EMF results (Eq. [7]) are indicated by the solid line in Fig. 4. For comparison, the calorimetric data, as assessed in Pankratz (1982), are indicated by the dashed line. Clearly the calorimetric data are not supported by either the EMF or the NiO + Ni-Pd redox sensor measurements, verifying our assertion that the previously determined enthalpy of formation for ReO_2 is in error.

The Re + ReO_2 oxygen fugacity buffer

The μO_2 defined by the Re + ReO_2 equilibrium has been determined to a high degree of accuracy using an electrochemical method with Ni + NiO and Cu + Cu_2O as reference electrodes. The internal consistency of the EMF measurements has been verified at $\approx$ 1.0 kbar pressure and between 800 and 1073 K using the NiO + Ni-Pd redox sensor technique. Hence the equilibrium between Re and ReO_2 provides a useable oxygen fugacity buffer in hydrothermal experiments which occurs mid-way between the NNO and HM (or MNO) buffers (Fig. 1). This is a region of f_{O_2} which is geologically significant. In the hydrothermal environment, RRO equilibrates rapidly, does not alloy significantly with any of the commonly used capsule materials (e.g. Au, Pt; Massalski 1986), and it has a large buffer capacity per unit volume, characteristics it shares with the more commonly used NNO buffer. Additionally, the increasingly frequent use of the relatively inert Re metal as a container for high T,P experimental charges imparts important design advantages including the potential for using the capsule itself to constrain f_{O_2}. This may be particularly significant in ultra-high pressure experiments where space considerations preclude the use of traditional double capsule buffer techniques.

Acknowledgments We are grateful to Fritz Seifert at the Bayerisches Geoinstitut for encouragement and financial support to pursue our studies of "redox reactions at high temperatures". Detlef Krauße (BGI) assisted with microprobe analyses, and Lee McRae (CSIRO) produced the final diagrams. Ian Grey, John Watts (both CSIRO) and I-Ming Chou provided helpful reviews. We also thank Werner Schreyer for his editorial handling.

References

Battles JE, Gunderson GE, Edwards RK (1968) A mass spectrometric study of the rhenium-oxygen system. J Phys Chem 72:3963–3969

Carmichael ISE (1991) The redox state of basic and silicic magmas: a reflection of their source regions? Contrib Mineral Petrol 106:129–141

Chou I-Ming (1987) Oxygen buffer and hydrogen sensor techniques at elevated pressures and temperatures. In: Ulmer GC, Barnes HC Jr (eds) Hydrothermal experimental techniques. Wiley, New York, pp 60–99

Eugster HP (1957) Heterogeneous reactions involving oxidation and reduction at high pressures and temperatures. J Chem Phys 26:1760–1761

Eugster HP, Wones DR (1962) Stability relations of the ferruginous biotite, annite. J Petrol 3:82–125

Franco JI, Kleykamp H (1971) Thermodynamics of the system Rhenium-Oxygen (in german). Ber Bunsenges Phys Chem 75:934–938

Hemingway BS (1990) Thermodynamic properties for bunsenite, NiO, magnetite, Fe_3O_4, and haematite, Fe_2O_3, with comments on selected oxygen buffer reactions. Am Mineral 75:781–790

Huebner JS (1971) Buffering techniques for hydrostatic systems at elevated pressures. In: Ulmer GC (ed) Research techniques for high pressure and high temperature. Springer-Verlag, Berlin Heidelberg New York, pp 123–178

Hultgren R, Desai PD, Hawkins DT, Gleiser M, Kelley KK, Wagman DD (1973) Selected values of the thermodynamic properties of the elements. Am Soc Met

Kerrick DM (1987) Cold-seal systems. In: Ulmer GC, Barnes HC Jr (eds) Hydrothermal experimental techniques, Wiley, New York, pp 293–323

King EG, Richardson DW, Mrazek RV (1969) Heats of formation of three oxides of rhenium. US Bur Mines Rep Invest 7323

Magnéli A (1957) Studies on rhenium oxides. Acta Chem Scand 11:28–33

Massalski TB (1986) Binary alloy phase diagrams, vols 1–2. Am Soc Met

O'Neill HStC (1988) Systems Fe-O and Cu-O: thermodynamic data for the equilibria Fe-"FeO," Fe-Fe_3O_4, "FeO"-Fe_3O_4, Cu-Cu_2O, and Cu_2O-CuO from EMF measurements. Am Mineral 73:470–486

O'Neill HStC, Pownceby MI (1993a) Thermodynamic data from redox reactions at high temperatures: zirconia electrolytes, with revised values for the Fe-"FeO", Co-CoO, Ni-NiO and Cu-Cu_2O oxygen buffers, and new data for the W-WO_2 buffer. Contrib Mineral Petrol 114:296–314

O'Neill HStC, Pownceby MI (1993b) Thermodynamic data from redox reactions at high temperatures. II. The MnO-Mn_3O_4 oxygen buffer, and implications for the thermodynamic properties of MnO and Mn_3O_4. Contrib Mineral Petrol 114:315–320

Pankratz LB (1982) Thermodynamic properties of elements and oxides. US Bur Mines Bull 672

Pownceby MI, O'Neill HStC (1994) Thermodynamic data from redox reactions at high temperatures. III. Activity-composition relations in Ni-Pd alloys from EMF measurements at 850–1250 K, and calibration of the NiO + Ni-Pd assemblage as a redox sensor. Contrib Mineral Petrol 116:327–339

Ramanarayan TA (1980) Limiting factors in measurements using solid electrolytes. In: Subbarao EC (ed) Solid electrolytes and their applications. Plenum Press, New York, pp 81–98

Rudert V, Chou I-M, Eugster HP (1976) Temperature gradients in rapid-quench cold-seal pressure vessels. Am Mineral 61:1012–1015

Stuve JM, Ferrante MJ (1976) Thermodynamic properties of rhenium oxides, 8 to 1400 K. US Bur Mines Rep Invest 8199

Taylor JR, Wall VJ, Pownceby MI (1992) The calibration and application of accurate redox sensors. Am Mineral 77:284–295